# Construction and optimization of multi-parameter cement strength numerical model based on percolation

**Wei Liu**
Hubei University of Technology
**Xuguang Wu** ( wuxu6661@outlook.com )
Hubei University of Technology https://orcid.org/0000-0003-4909-918X
**Yingbin Wang**
Hubei University of Technology
**Zhiwei Ye**
Hubei University of Technology
**Pan Li**
Hubei University of Technology

**Research Article**

**Keywords:** percolation, cement strength, porosity, lightning search algorithm

**Posted Date:** April 13th, 2022

**DOI:** https://doi.org/10.21203/rs.3.rs-1528416/v1

# Construction and optimization of multi-parameter cement strength numerical model based on percolation

**Wei Liu [1], Xuguang Wu[1], Yingbin Wang[2], Zhiwei Ye[1],Pan Li[1]**
[1]School of Computer Science, Hubei University of Technology, Wuhan, 430000,China
[2]School of Civil Engineering, Architecture and Environment, Hubei University of Technology
Corresponding author: Xuguang Wu (e-mail:wuxu6661@outlook.com)

**Abstract:** The prediction of the mechanical properties of different dosages amounts of cement has been a hot topic in various scholars. In addition to water and a small amount of air and pores, cement has unhydrated cementitious material particles and hydration products. It was found that the hydration products CH and C-S-H gel in cement had certain effects on the mechanical properties of cement. In the theory of many porosity and cement mechanical properties, the theory of porosity and cement mechanical properties based on percolation theory can better predict the strength of cement stone. This paper studies the hydration products on cement,a numerical model of multi-parameter cement mechanical properties based on porosity and hydration products was proposed. By using various optimization algorithms to fit and optimize the constructed numerical model, it was found through multiple experiments and comparisons. The lightning search algorithm can achieve a certain effect on the optimized fitting of the constructed mathematical model. The multi-parameter numerical model based on pore percolation constructed in this paper is well fitted. In terms of predicting cement strength, it is superior to the three most cited porosity strength models at home and abroad and the porosity strength model based on percolation theory.
***Keyword**: percolation; cement strength; porosity; lightning search algorithm;*

## 1. Introduction

Percolation theory is one of the best theoretical methods for dealing with systems with strong disorder and random geometry (J. Zallen, R. (2007)). It provides a clear and intuitive model for describing spatial stochastic processes and can be applied to a wide range of physical phenomena. The term percolation was created by mathematician J M Hammersley in 1957 ( Hammersley J M, Handscomb D C(1957))when fluids were flowed in a network of disordered multi-channels (but some channels were randomly blocked), now percolation Theory has become the classic theory for dealing with the effects of changes in the degree of linkage in disordered systems.

In order to explain the interaction between various components in cement-based materials and their relationship with macroscopic properties. The centroplasm hypothesis is to divide the phase of the cement stone into a central (dispersion phase) and a medium (continuous phase) at different levels. In the centroplasm hypothesis describing the relationship between the microstructure and macroscopic properties of cement, the central effect is used. Describe the interaction of the various phases in the cement stone (the centroplasm and the medium), and the centroplasm effect can be regarded as a simple understanding of the spatial coupling characteristics of each phase in the random stone structure in the cement stone microstructure. Although the centroplasm hypothesis has successfully explained the relationship between the microstructure and properties of cement-based materials, it is not possible to quantitatively or semi-quantitatively guide the design of cement-based materials. The percolation theory can at least semi-quantitatively determine the centroplasm hypothesis. The theoretical analysis of percolation of cement stone microstructure shows that the pore part has no strength and is dispersed and degraded. The existence of pores will strongly affect the strength of cement stone. Especially in the case of pore percolation, the macroscopic performance of cement is usually expressed as porosity. There is a good correlation.

At present, the most widely used theory of cement stone strength is the porosity theory. Because the pore is the non-strength part of the cement stone, the porous nature of the cement-based material makes the influence of the porosity on its strength particularly prominent, which makes the model agree well with the experimental results to a certain extent, and the porosity model easy to calculate, which is why porosity theory is respected. For a long time, more than ten semi-empirical formulas describing the relationship between porosity and strength have been established, the most representative of which are the following: Balshin formula, Ryshkevitch formula and Schiller formula (Kearsley E P, Wainwright P J (2002); Pandey S P, Sharma R L (2000)), but the above models are in different range of porosity. The regression range of the rate range is good for the experimental data. The deviation from this range is also large, and the correlation of the porosity-strength model fitting based on the percolation theory constructed by He Xingyang and other scholars in 2009 (Baoguo Ma (2005); Yongxin Li (2003)) is better than the current application 3 models. Calculating the strength of cement through porosity has always been a hot spot for scholars (Grabois T M, Cordeiro G C, Filho R D T(2018); Zajac M, Skocek J, Adu-Amankwah S, et al (2018)).

Cement stone is usually composed of unhydrated cementitious material particles, hydration products, water and a small amount of air, and pores occupied by water and air. ( Peng Zhao,WeiHe Wang (2008); Zhao Z, Du C W, Shen L(2013)) The mechanical properties of cement stone depend mainly on the nature, relative content of these components and the interaction between them. Calcium hydroxide (CH) is an important cement hydration product, its composition and structure directly affect the structure and properties of cement stone. In the strength of cement, because it can block the crack propagation, and at the same time play a certain skeleton role to conduct stress has a certain positive effect on the strength. The hydrated calcium silicate gel is the main product of silicate cement hydration production. Due to the complexity of its own

structure, direct quantitative analysis of the gel is difficult. If it is assumed that the composition change of C-S-H is not too large, the amount of gel in the different hydration products can be roughly evaluated by the amount of water of the thermally analyzed gel-bound water. The cement hydration process is essentially a process of combining water, and the combination of water content and type is also a factor affecting the microstructure of the cement(Constantinides G, Ulm F J(2004); Wang L, Yang H Q, Zhou S H, et al (2018); Land G, Stephan D(2018); Borges P H R, Costa J O, Milestone N B, et al(2010)).

The porosity strength model based on percolation theory, this paper studies the CH content and combined water content of various blends with different dosages at different times.At present, artificial intelligence algorithms are used in various fields, especially in the optimization design of various models(M. Elsisi(2022);Mahmoud Elsisi,Minh-Quang Tran,Hany M. Hasanien,Rania A. Turky,Fahad Albalawi,Sherif S. M. Ghoneim(2021);M. Elsisi,Mohamed A. Ebrahim(2021)).In this paper, a new multi-parameter cement strength model based on percolation theory for porosity, gel-bound water, total combined water, and CH is proposed.The lightning search algorithm(SHAREF H,IBRAHIM A A, MUTLAG A H(2015))is a new heuristic optimization algorithm proposed by Shareef H in 2015 based on the natural phenomenon of lightning. Compared with the traditional algorithm, the algorithm has fast convergence speed and good optimization effect. Many scholars seek to get the optimal solution by using the algorithm in various fields(Ammar M, Mohamed A, Abubarkr H(2020); Mohammed W,Awartni-Ghaith M,Oujda K(2020);Ashish-Kumar B, Neha- Singh, Immadisetty-Vinod K(2020);ArupRantan, AjoyKumar - Chakraborty(2019) ; W.M.Hamanah, M.A.Abido, Luai M(2019); M.Elsisi, H. Abdelfattah(2020); Serhat Duman(2019)). In this paper, the lightning search algorithm is used to optimize the fit of the constructed cement stone strength model, so that the model can achieve better prediction results.

## 2. Model construction and optimization

### 2.1 Research on model background

Among the many theories of cement stone strength, the most widely used theory is the porosity theory of cement stone. Because the pores do not have strength in the cement stone, the porosity has a direct influence on the strength of the cement. The resulting model of cement stone and porosity is also close to the experimental results. For a long time, more than ten semi-empirical formulas describing the relationship between porosity and strength have been established. The most representative models are the Balshin formula, the Ryshkevitch formula, and the Schiller formula. The following table shows the various formulas and descriptions, where P represents porosity and σ represents cement stone strength.

**Table 1** Classical Formula of Porosity and Strength

| Formula | SPR position, nm | FWHM, nm |
|---|---|---|
| Balshin | $\sigma=\sigma_0\cdot(1-P)^A$ | A is a constant, $\sigma_0$ is the cement stone strength when the porosity is zero. |
| Ryshkevitch | $\sigma=\sigma_0\cdot e^{-BP}$ | B is a constant, $\sigma_0$ is the cement stone strength when the porosity is zero. |
| Schiller | $\sigma=C\cdot In(P_{cr}/P)$ | C is a constant, and $P_{cr}$ is the porosity when the cement stone strength is zero. |

The strength and porosity of cement stone have a high correlation, and the above porosity models all have certain errors in different porosity ranges. Schiller confirmed that the Ryshkevitch formula and the Schiller formula are only slightly different at the two extreme porosity, the Ryshkevitch formula is more accurate at low porosity, and the Schiller formula is more accurate at higher porosity. That is to say, the predicted values of the two formulas in different porosity ranges are larger than the actual values, and the changes of the strength with the fluctuation of the porosity cannot be well reflected.

He Xingyang and other scholars proposed a cement microstructure model based on percolation theory. The pores in the cement stone do not have strength, which is the degraded phase in the cement stone, so that the strength of the cement stone is much lower than the bonding strength of the silicate structure; and the hole is usually due to the failure of the original water filling space in the cement slurry. The formation of the product is filled to a certain extent, reflecting the degree of hydration products such as C-S-H gel. The distribution and coupling of pores in space will affect the strength of cement stone. In ordinary cement stone, the porosity (pore fractional volume) generally exceeds the percolation threshold of 0.16 in three-dimensional space, and the percolation path of the pore has appeared, which makes the cement stone show a certain pore property in the macroscopic view, so the macroscopic mechanics of ordinary cement stone, the performance is mainly related to the spatial coupling degree of the holes. Therefore, when constructing the cement stone strength porosity model, the degree of the hole close to the percolation should be reflected in the mathematical analytical formula, that is, the closeness of the pore fraction volume (porosity) and its percolation threshold. Based on the above analysis of pore percolation and numerical analysis, He Xingyang and other scholars constructed a function $f(P)$ that reflects the extent to which the pores are close to percolation, $f(P)$ is defined as Eq. (1):

$$f(P)=\frac{P_{cr}^2-P}{P_{cr}^2-P_{cr}^3} \tag{1}$$

Where: $P$ is the porosity of cement stone

$P_{cr}^2$ is the percolation threshold on a two-dimensional plane

$P_{cr}^3$ is the percolation threshold in the third degree space

The function $f(P)$ is the ratio of the percolation threshold of the hole in the two-dimensional space to the porosity P of the cement stone. The ratio of the difference between the percolation threshold of the hole in the two-dimensional space and the three-dimensional space, $f(P)$ reflects the cement stone. The mesopores are far from the critical region of the percolation flow on the two-dimensional plane, and close to the critical state of the percolation path in the three-dimensional space. In addition, the function value of the function $f(P)$ also satisfies the requirement of amplifying the change in the porosity $P$ value.

The percolation theory holds that the nature of the system exhibits different forms of exponential function changes in the neighborhood of its percolation threshold, and a cement stone strength porosity model of the following formula is constructed, $\sigma$ is defined as Eq. (2):

$$\sigma = \sigma_0 \cdot [f(P)]^n = \sigma_0 \cdot (\frac{P_{cr}^2 - P}{P_{cr}^2 - P_{cr}^3})^n \quad (2)$$

Where: σ is cement stone strength

$P$ is cement stone porosity

$P_{cr}^2$ is the percolation threshold on a two-dimensional plane, and the value is 0.47.

$P_{cr}^3$ is the percolation threshold in three dimensions, with a value of 0.16

$\sigma_0$ is the critical point of cement stone strength in the three-dimensional space where the percolation path appears.

$n$ is the influence of the degree $f(P)$ of the hole away from the two-dimensional percolation and the three-dimensional percolation on the strength of the cement stone. When $P \geq 0.47$ or $f(P) \leq 0$, the randomly distributed pores have a seepage path on any plane in the cement stone structure. Through any plane in the cement stone, the cement stone has become a fragmented structure, mechanical properties. The mesh structure can no longer function and is scattered, so the cement stone does not have strength; when $P < 0.16$ or $f(P) > 1$, the hole does not see a seepage path in the cement stone, and the strength of the cement stone is mainly determined by the cement. The properties of the other phases in the stone, the spatial coupling degree and the distribution characteristics, the variation of the fractional volume of the pores in this region has no significant effect on the cement stone strength; when $0.16 \leq P \leq 0.47$, $f(P)$ takes [0, 1] When the value is in the interval, the joint state of the hole in the cement stone space is between the three-dimensional seepage critical point and the two-dimensional seepage critical point. The hole has a seepage path in the three-dimensional space of the cement stone, and the fractional volume change of the hole has the performance of the cement stone. Has a strong influence. What is reflected is the relationship between porosity and strength in the range of porosity.

Because the original porosity strength model can not reflect the severity of the influence of porosity fluctuation on cement stone strength in a large porosity range, the error is relatively large. The constructed percolation-based porosity strength model can accurately reflect the relationship between cement stone strength and porosity. However, through experiments and calculations, although the porosity strength model proposed above can reflect the large change in strength caused by the porosity fluctuation, the theoretical and actual values calculated for some cement stone models with blends are different.

## 2.2 Multi-parameter numerical model construction based on percolation

According to the cement stone microstructure model based on percolation theory, cement stone consists of dispersion-enhanced phase (crystalline phase such as CH, AFt, unhydrated particles), dispersed degraded phase (pore, micro-crack) and continuous phase (CSH gel, etc.) And so on.

CH is an important cement hydration product, its composition and structure directly affect the structure and properties of cement stone. From the strength investigation, on the one hand, it is the weak link of the cement stone due to its interface orientation, cleavage and its own defects. On the other hand, it can block the crack propagation and at the same time play a certain skeleton to conduct the stress and strength. Certainly positive effects; from the durability investigation, CH with excessive dissolution performance will reduce the resistance of cement stone to solution erosion, but when CH is too small, it will affect the stable existence of other hydration products. In reinforced concrete, certain CH is still The necessary conditions to ensure that the steel bars are protected from rust.

Gel-bound water can be used to evaluate the promoting effect of the auxiliary gelling material on the formation of C-S-H gel. The dispersion-enhanced phase bodies generally have higher strength, but there is almost no bonding between them. There is a large amount of cementation transition layer composed of CSH gel and the like between the dispersion-enhancing phases, and the transition layer is hydrated. The crystalline phase and the unhydrated particles act as a series of physical, chemical and physical chemical interactions such as bonding, mechanical occlusion, encapsulation, compounding and adsorption, so that the cement stone forms a whole and has strength.

The hydration process of cement is essentially a process of continuously combining water, so the total amount of combined water can relatively assess the hydration process of different systems. The total amount of water combined with the hydration product can be used to assess the degree of hydration of the system, and the deeper the degree of hydration, the higher the macroscopic mechanical properties of the system.

The pores in the cement are basically free of mechanical properties. The porosity as the dispersed degraded phase has a direct influence on the cement strength, while the CH, the gel-bound water and the total bound water as the dispersion enhance the mechanical properties of the cement.

Through a large number of experiments and derivations, the multi-parameter strength model based on the percolation theory of porosity, gel-bound water, total combined water, and CH is obtained, $\sigma$ is defined as Eq. (3):

$$\sigma = \left( w1 \cdot C + w2 \cdot \left( \frac{Pl}{Pz} \right) \right) \cdot [f(P)]^n = \left( w1 \cdot C + w2 \cdot \left( \frac{Pl}{Pz} \right) \right) \cdot \left( \frac{P_{cr}^2 - P}{P_{cr}^2 - P_{cr}^3} \right)^n \quad (3)$$

In the formula:

$\sigma$ is cement stone strength

$P$ is cement stone porosity

$P_{cr}^2$ is the percolation threshold on a two-dimensional plane, and the value is 0.47.

$P_{cr}^3$ is the percolation threshold in three dimensions, with a value of 0.16

$n$ is the influence of the degree $f(P)$ of the hole away from the two-dimensional percolation and the three-dimensional percolation on the strength of the cement stone

$w1$ , $w2$ are weighting constants

$C$ is the CH content

$Pl$ is the gel-bound water content

$Pz$ is the total combined water content

Compared with the porosity-cement strength model based on pore seepage, the multi-parameter model constructed in this paper not only reflects the critical extent of the pores away from the critical region of seepage in the two-dimensional plane, but also the critical state of the seepage in the three-dimensional space. That is, the influence of $f(P)$ on the strength σ of cement stone. At the same time, by considering the influence of the hydration product CH in the cement hydration process and the C-S-H gel expressed by the gel-bound water on the cement strength, considering more factors, it can be better reflected than the single porosity. The relationship between the mechanical properties exhibited by the microstructure of the cement and the macrostructure of the cement.

## 2.3 Optimization analysis of model using optimization algorithm

The lightning search algorithm is a new heuristic optimization algorithm proposed by Hussain Shareef in 2015. The algorithm is derived from the natural phenomenon of lightning. The random distribution function is created to solve the problem to be optimized through the discharge probability characteristics and tortuous characteristics of the transition discharge body, the space discharge body and the guide discharge body.

The lightning search algorithm can be summarized as: the lightning fast particle of the cascade pilot propagation mechanism is defined as the discharge body, and the concept of the discharge body is similar to the terms "particle" or "individual" used in the PSO ; it is assumed that each discharge body contains one step The leader and a channel, the number of transitional discharge bodies represents the initial population size, and each individual discharge body represents a set of spatial random candidate solutions to be optimized; the spatial optimal solution of the problem to be optimized is the current maximum energy guidance. The top position where the discharge body is located.

The speed of the projectile can be expressed as Eq. (4):

$$v_p = [1 - (\frac{1}{\sqrt{1-(v_0/c)^2}} - \frac{sF}{mc^2})^{-2}]^{-1/2} \quad (4)$$

Where: $v_p$ and $v_0$ are the current velocity and initial velocity of the projectile; c is the speed of light; $F$ is the constant ionization rate; m is the mass of the projectile; $s$ is the length of the path that passes.

Equation (4) shows that: speed is a function of the position energy of the leading tip and the mass of the projectile. When the mass is small or the path is long, the projectile has almost no potential to ionize or detect large space. It can only ionize or develop nearby space. Therefore, the LSA's exploration and development capabilities can be controlled by the relative energy of the cascade leader. Another important feature of the projectile is the bifurcation, which is achieved by creating a symmetric channel, see Eq. (5):

$$\overline{p_i} = a + b - p_i \quad (5)$$

Where: $\overline{p_i}$ , $p_i$ are the two opposite shots in the one-dimensional problem; a and b are the range boundaries, respectively.

Discharge body modeling and cascade pilot movement

1. Transition discharge body. Let a cascade pilot with group size $N$ be $sl$ = [ $sl_1$ , $sl_2$ , ..., $sl_n$ ], which satisfies the position of the $N$ random discharge bodies $P_t$ of the solution to be optimized, denoted as $P_t$ = [ $P_{t1}$ , $P_{t2}$ , ..., $P_{tn}$ ]. . The probability density function $f(x^T)$ of the transitional discharge body is created from the random space representing the solution space using the standard uniform distribution probability. The standard uniform distribution probability density function $f(x^T)$ can be expressed as Eq. (6):

$$(x^T) = \begin{cases} \frac{1}{b} - a, a \le x^T \le b; \\ 0, x < a \text{或} x^T > b. \end{cases} \quad (6)$$

Where: $x^T$ is the random number of the initial tip energy $Esl_i$ that can provide the candidate solution or the step leader $sl_i$ ; a and b are the boundary ranges of the solution space, respectively.

2. Space discharge body. Let the position of the space discharge body be $Ps$ =[ $ps_1$ , $ps_2$ , ..., $ps_n$ ], mathematically model the random number generated by the exponential distribution function with shape parameter $\mu$ , and the exponential distribution probability density function $f(x^S)$ is given as Eq. (7):

$$f(x^S)=\begin{cases}\frac{1}{\mu}e^{-\frac{x^S}{\mu}}, x^S \geq 0;\\ 0, x^S < 0.\end{cases} \tag{7}$$

Equation (7) shows that the position of the space discharge body or the direction of the next iteration can be controlled by the shape parameter $\mu$ . In the LSA, $\mu_i$ is the distance between the pilot discharge body PL and the spatial discharge body $ps_i$ . According to this definition, $ps_i$ can be described as the $t+1$ th iteration:

$$ps_{i\_now} = ps_i \pm \exp(rand(\mu_i)) \tag{8}$$

Where $\exp(rand())$ is a random index.

3. Guide the discharge body. Mathematical modeling is performed using a random number generated by a standard normal distribution with a shape parameter $\mu$ and a scale parameter $\sigma$ , whose normal probability density function $f(x^L)$ is expressed as Eq. (9):

$$f(x^L)=\frac{1}{\sigma\sqrt{2\pi}}e^{-\frac{(x^L-\mu)^2}{2\sigma^2}} \tag{9}$$

Equation (9) shows that: The randomly generated guided discharge body can be searched from all directions of the current position defined by the shape parameter, and its mining capacity can be defined by the scale parameter. The pilot discharge body $PL$ can be described at the $t+1$ th iteration position as Eq. (10):

$$pL_{i\_new} = pL_i \pm norm(rand(\mu_L\sigma_L)) \tag{10}$$

Where $norm(rand(\mu_L\sigma_L))$ is a random number generated by a normal distribution function.

The lightning search algorithm is quite similar to some traditional optimization algorithms, with strong global optimization ability, high convergence precision and few adjustment parameters.

The steps of the lightning search algorithm can be summarized as the following steps:

Step1: Initialize the number of iterations, the number of channel attempts, the size of the bomb population

Step2: Randomly generate *N* gradient pilots (transition bombs)

Step3: Evaluate performance by the energy *Ep* of the pellet

Step4: Update the gradient leader energy $Es_1$ , update the best and worst pilots

Step5: When the maximum number of channel attempts is reached, replace the worst pilot with the best pilot, and reset the number of channel attempts to adjust the search direction of the marble. If the maximum number of channel attempts is not reached, directly adjust the search direction of the projectile.

Step6: Jet space pellets and leading pellets

Step7: Evaluate performance by the energy *Ep* of the bomb, update the gradient pilot

Step 8: If the maximum number of iterations is reached, a gradient leader is returned, and the maximum number of iterations is not reached, and the third step is returned to continue the iteration.

The multi-parameter model constructed in this paper is fitted by lightning search algorithm, and the constructed multi-parameter model is trained by the experimentally measured data. The optimization algorithm can obtain a better result through a large amount of data training. There are not many training samples in this paper. Many optimization algorithms do not converge on the square root error because of too few training samples, or can not get the optimal solution, like the fruit fly optimization used in the experiment. The algorithm can't converge at all. It is difficult to get the optimal solution as the genetic algorithm of the contrast experiment. However, the lightning search algorithm can converge quickly under the condition of a small number of samples, and the overall search ability is strong.

The lightning search algorithm is used to first initialize the number of iterations, the number of channel attempts, and the size of the pellet population. The root mean square error of the cement stone strength calculated by the model constructed in this paper and the actual strength of the cement stone measured by the experiment is used as the fitness function of the lightning search, and the optimal solution is found by iteration.

**Table 2** Formula obtained by optimization

| | LSA | GA |
|---|---|---|
| Overall data | $\sigma=(1.58\cdot C+43.98\cdot(\frac{Pl}{Pz}))\cdot[f(P)]^{0.456}$ | $\sigma=(1.12\cdot C+57.57\cdot(\frac{Pl}{Pz}))\cdot[f(P)]^{0.597}$ |

| | | |
|---|---|---|
| OPC | $\sigma = (0.18 \cdot C + 73.66 \cdot (\frac{Pl}{Pz})) \cdot [f(P)]^{0.359}$ | $\sigma = (0.11 \cdot C + 75.61 \cdot (\frac{Pl}{Pz})) \cdot [f(P)]^{0.356}$ |
| Different dosages amount of steel slag | $\sigma = (1.58 \cdot C + 39.84 \cdot (\frac{Pl}{Pz})) \cdot [f(P)]^{0.336}$ | $\sigma = (1.84 \cdot C + 32.36 \cdot (\frac{Pl}{Pz})) \cdot [f(P)]^{0.314}$ |
| Different dosages amount of slag | $\sigma = (0.95 \cdot C + 54.9 \cdot (\frac{Pl}{Pz})) \cdot [f(P)]^{0.495}$ | $\sigma = (0.6 \cdot C + 65.19 \cdot (\frac{Pl}{Pz})) \cdot [f(P)]^{0.51}$ |
| Different dosages amount of fly ash | $\sigma = (-2.31 \cdot C + 154.52 \cdot (\frac{Pl}{Pz})) \cdot [f(P)]^{0.85}$ | $\sigma = (92.35 \cdot (\frac{Pl}{Pz})) \cdot [f(P)]^{0.7}$ |

## 3. Experiment and analysis

### 3.1 Experimental Design

In the experimental verification, a total of 13 sets of experiments were designed. The experiment used Yanshan Portland cement. In addition to pure cement, it also considered the admixture of cement mixed with different minerals. CH, gel-bound water, total bound water, Porosity and strength. Three different mineral admixtures were used in the experiment: 400m2/kg WISCO steel slag, 400m2/kg Shougang slag and 460m2/kg Shijingshan second-grade fly ash. A total of four levels of 10%, 20%, 30%, and 40% of various mineral admixtures were set, and the data were measured for 3 days, 7 days, 28 days, 90 days, and 180 days. In the cement number of the table, OPC refers to pure cement without any admixture, while SL refers to cement with slag, ST refers to cement with steel slag, FA It refers to cement mixed with fly ash. The water to cement ratio of the paste is 0.44.

**Table 3** The proportion of cementitious materials (%）

| Identifier | OPC | ST1 | ST2 | ST3 | ST4 | SL1 | SL2 | SL3 | SL4 | FA1 | FA2 | FA3 | FA4 |
|---|---|---|---|---|---|---|---|---|---|---|---|---|---|
| Cement | 100 | 90 | 80 | 70 | 60 | 90 | 80 | 70 | 60 | 90 | 80 | 70 | 60 |
| Steel slag | / | 10 | 20 | 30 | 40 | / | / | / | / | / | / | / | / |
| Sag | / | / | / | / | / | 10 | 20 | 30 | 40 | / | / | / | / |
| Fly ash | / | / | / | / | / | / | / | / | / | 10 | 20 | 30 | 40 |

The hardening slurry porosity and the strength of the mortar of the above 13 groups were measured at 3 days, 7 days, 28 days, 90 days and 180 days.

**Table 4** Cement stone porosity and mortar strength

| Identifier | Amount blend | porosity (%) | | | | | Cement strength (MPa) | | | | |
|---|---|---|---|---|---|---|---|---|---|---|---|
| | | 3d | 7d | 28d | 90d | 180d | 3d | 7d | 28d | 90d | 180d |
| C0 | 0% | 38.11 | 31.85 | 21.76 | 20.64 | 20.81 | 35.8 | 45.4 | 54.4 | 55.2 | 57.6 |
| ST1 | 10% | 37.07 | 32.57 | 23.54 | 20.51 | 21.37 | 33.3 | 43.2 | 54.4 | 60.0 | 63.6 |
| ST2 | 20% | 40.53 | 35.89 | 26.38 | 24.22 | 22.86 | 29.6 | 42.7 | 50.0 | 60.0 | 60.1 |
| ST3 | 30% | 41.77 | 37.03 | 29.67 | 26.36 | 25.82 | 23.5 | 38.1 | 47.1 | 57.6 | 58.8 |
| ST4 | 40% | 44.95 | 40.16 | 32.82 | 29.55 | 29.63 | 18.1 | 32.1 | 44.1 | 54.2 | 57.9 |
| SL1 | 10% | 39.67 | 30.89 | 21.36 | 18.98 | 18.18 | 36.3 | 46.6 | 60.3 | 60.4 | 59.7 |
| SL2 | 20% | 32.80 | 24.46 | 15.59 | 12.96 | 12.04 | 29.1 | 41.8 | 56.4 | 61.8 | 61.8 |
| SL3 | 30% | 35.77 | 32.70 | 20.01 | 17.05 | 17.05 | 23.3 | 37.5 | 54.2 | 68.1 | 68.8 |
| SL4 | 40% | 42.74 | 34.36 | 21.35 | 18.62 | 18.36 | 19.7 | 34.8 | 52.0 | 69.0 | 69.8 |
| FA1 | 10% | 38.86 | 32.08 | 23.34 | 21.48 | 20.32 | 31.0 | 40.0 | 47.6 | 64.7 | 66.4 |
| FA2 | 20% | 39.83 | 33.44 | 26.72 | 24.03 | 23.99 | 24.4 | 32.4 | 45.8 | 63.3 | 71.6 |
| FA3 | 30% | 41.12 | 36.10 | 29.30 | 26.95 | 26.81 | 20.5 | 28.8 | 41.6 | 59.2 | 70.3 |

| | | | | | | | | | | | |
|---|---|---|---|---|---|---|---|---|---|---|---|
| FA4 | 40% | 42.93 | 38.19 | 33.03 | 31.13 | 31.19 | 12.9 | 20.8 | 33.3 | 46.1 | 55.7 |

Gel-bound water, CH, total bound water of the hydration product of the composite system calculated by thermal analysis.

**Table 5** CH of hydration products of composite system

| Identifier | Amount of blend | CH quantitative analysis results(%) | | | | |
|---|---|---|---|---|---|---|
| | | 3d | 7d | 28d | 90d | 180d |
| C0 | 0% | 15.43 | 18.03 | 21.65 | 20.62 | 21.21 |
| ST1 | 10% | 14.94 | 17.13 | 20.76 | 19.69 | 23.06 |
| ST2 | 20% | 14.10 | 15.52 | 20.21 | 20.28 | 23.05 |
| ST3 | 30% | 13.67 | 15.50 | 20.18 | 19.64 | 22.01 |
| ST4 | 40% | 13.12 | 15.48 | 19.84 | 18.47 | 21.60 |
| SL1 | 10% | 14.18 | 12.57 | 19.44 | 18.90 | 20.16 |
| SL2 | 20% | 12.96 | 14.67 | 16.32 | 14.61 | 15.95 |
| SL3 | 30% | 12.51 | 13.77 | 14.22 | 15.41 | 15.91 |
| SL4 | 40% | 11.82 | 12.57 | 12.77 | 12.05 | 13.99 |
| FA1 | 10% | 14.43 | 17.12 | 18.60 | 18.87 | 19.69 |
| FA2 | 20% | 13.69 | 16.01 | 17.59 | 17.52 | 18.14 |
| FA3 | 30% | 12.84 | 14.92 | 15.96 | 16.08 | 14.94 |
| FA4 | 40% | 11.80 | 12.91 | 14.65 | 13.90 | 12.43 |

## 3.2 Analysis

Using the multi-parameter model constructed in this paper, the data in the above table is substituted into the model to calculate the compressive strength of the cement. The original single-parameter model was compared with a multi-parameter model optimized using lightning search algorithm and genetic algorithm, respectively. At the same time, the obtained values are compared with the three empirical formulas currently used: Blashin formula, Ryshkevitch and Schiller formula.

The following table shows the theoretical values obtained by using the single-parameter model and the multi-parameter model optimized by genetic algorithm, using the multi-parameter model optimized by the lightning search algorithm, and calculating the calculated theoretical values and the actual data obtained from the experiment. The percentage error ratio is exceeded.

**Table 6** Multi-parameter model fitting model calculation results

| Identifier | Experimental data | Single parameter | Single parameter percentage error | Multiple parameters (GA) | Multiple parameter percentage error(GA) | Multiple parameters (LSA) | Multiple parameter percentage error(LSA) |
|---|---|---|---|---|---|---|---|
| C0 | 35.8 | 31.10 | -15.10% | 31.95 | -12.06% | 31.83 | -12.48% |
| C0 | 45.4 | 42.77 | -6.16% | 43.43 | -4.54% | 43.85 | -3.53% |
| C0 | 54.4 | 58.01 | 6.23% | 58.27 | 6.64% | 60.90 | 10.67% |
| C0 | 55.2 | 59.54 | 7.28% | 59.74 | 7.60% | 60.89 | 9.34% |
| C0 | 57.6 | 59.31 | 2.88% | 59.52 | 3.23% | 62.51 | 7.86% |
| SS | 33.3 | 33.23 | -0.21% | 34.05 | 2.20% | 33.30 | 0.00% |
| SS | 43.2 | 41.54 | -3.99% | 42.23 | -2.30% | 41.71 | -3.58% |
| SS | 54.4 | 55.53 | 2.04% | 55.86 | 2.62% | 57.68 | 5.69% |

| | | | | | | | |
|---|---|---|---|---|---|---|---|
| SS | 60 | 59.71 | -0.48% | 59.91 | -0.15% | 59.92 | -0.13% |
| SS | 63.6 | 58.55 | -8.63% | 58.78 | -8.19% | 62.94 | -1.05% |
| SS | 29.6 | 25.73 | -15.05% | 26.61 | -11.26% | 25.94 | -14.12% |
| SS | 42.7 | 35.53 | -20.16% | 36.32 | -17.55% | 34.82 | -22.63% |
| SS | 50 | 51.41 | 2.75% | 51.86 | 3.59% | 53.53 | 6.59% |
| SS | 60 | 54.57 | -9.96% | 54.93 | -9.24% | 56.71 | -5.80% |
| SS | 60.1 | 56.49 | -6.39% | 56.79 | -5.83% | 61.01 | 1.49% |
| SS | 23.5 | 22.66 | -3.72% | 23.54 | 0.16% | 23.72 | 0.91% |
| SS | 38.1 | 33.31 | -14.38% | 34.13 | -11.64% | 33.89 | -12.42% |
| SS | 47.1 | 46.34 | -1.63% | 46.92 | -0.38% | 49.13 | 4.12% |
| SS | 57.6 | 51.44 | -11.97% | 51.89 | -11.00% | 53.08 | -8.51% |
| SS | 58.8 | 52.24 | -12.55% | 52.67 | -11.64% | 55.79 | -5.40% |
| SS | 18.1 | 12.95 | -39.77% | 13.73 | -31.88% | 15.05 | -20.26% |
| SS | 32.1 | 26.60 | -20.69% | 27.47 | -16.85% | 28.10 | -14.24% |
| SS | 44.1 | 41.11 | -7.27% | 41.80 | -5.49% | 44.10 | 0.00% |
| SS | 54.2 | 46.53 | -16.47% | 47.11 | -15.05% | 47.66 | -13.71% |
| SS | 57.9 | 46.41 | -24.77% | 46.99 | -23.23% | 50.05 | -15.67% |
| SL | 36.3 | 27.72 | -30.96% | 28.59 | -26.98% | 28.39 | -27.85% |
| SL | 46.6 | 44.37 | -5.04% | 44.99 | -3.57% | 41.63 | -11.95% |
| SL | 60.3 | 58.56 | -2.97% | 58.80 | -2.56% | 59.46 | -1.41% |
| SL | 60.4 | 61.75 | 2.18% | 61.88 | 2.39% | 61.11 | 1.16% |
| SL | 59.7 | 62.79 | 4.93% | 62.89 | 5.08% | 63.90 | 6.57% |
| SL | 29.1 | 41.14 | 29.27% | 41.84 | 30.45% | 37.33 | 22.04% |
| SL | 41.8 | 54.22 | 22.91% | 54.59 | 23.43% | 48.82 | 14.38% |
| SL | 56.4 | 66.11 | 14.68% | 66.09 | 14.66% | 61.20 | 7.85% |
| SL | 61.8 | 69.36 | 10.90% | 69.22 | 10.72% | 61.80 | 0.00% |
| SL | 61.8 | 70.47 | 12.31% | 70.29 | 12.08% | 64.74 | 4.55% |
| SL | 23.3 | 35.76 | 34.85% | 36.55 | 36.25% | 33.25 | 29.92% |
| SL | 37.5 | 41.32 | 9.24% | 42.01 | 10.73% | 38.87 | 3.53% |
| SL | 54.2 | 60.38 | 10.24% | 60.56 | 10.50% | 55.28 | 1.96% |
| SL | 68.1 | 64.25 | -5.99% | 64.30 | -5.91% | 58.99 | -15.45% |
| SL | 68.8 | 64.25 | -7.08% | 64.30 | -7.00% | 60.56 | -13.61% |
| SL | 19.7 | 20.04 | 1.72% | 20.91 | 5.81% | 21.00 | 6.20% |
| SL | 34.8 | 38.20 | 8.90% | 38.95 | 10.65% | 35.88 | 3.01% |
| SL | 52 | 58.57 | 11.22% | 58.81 | 11.58% | 52.63 | 1.19% |
| SL | 69 | 62.22 | -10.90% | 62.34 | -10.69% | 54.41 | -26.82% |
| SL | 69.8 | 62.56 | -11.57% | 62.67 | -11.38% | 57.40 | -21.59% |
| FA | 31 | 29.51 | -5.05% | 30.37 | -2.09% | 30.03 | -3.22% |
| FA | 40 | 42.38 | 5.61% | 43.05 | 7.08% | 42.52 | 5.94% |
| FA | 47.6 | 55.81 | 14.72% | 56.14 | 15.21% | 55.70 | 14.53% |
| FA | 64.7 | 58.40 | -10.80% | 58.64 | -10.34% | 58.25 | -11.07% |
| FA | 66.4 | 59.97 | -10.73% | 60.16 | -10.37% | 61.21 | -8.48% |
| FA | 24.4 | 27.36 | 10.81% | 28.23 | 13.56% | 27.60 | 11.60% |
| FA | 32.4 | 40.03 | 19.05% | 40.74 | 20.47% | 39.45 | 17.88% |
| FA | 45.8 | 50.90 | 10.03% | 51.37 | 10.84% | 50.69 | 9.65% |
| FA | 63.3 | 54.84 | -15.43% | 55.19 | -14.70% | 54.09 | -17.02% |

| | | | | | | | |
|---|---|---|---|---|---|---|---|
| FA | 71.6 | 54.89 | -30.43% | 55.24 | -29.60% | 54.84 | -30.56% |
| FA | 20.5 | 24.30 | 15.64% | 25.18 | 18.59% | 24.52 | 16.38% |
| FA | 28.8 | 35.13 | 18.02% | 35.93 | 19.84% | 34.35 | 16.16% |
| FA | 41.6 | 46.93 | 11.36% | 47.50 | 12.42% | 45.72 | 9.01% |
| FA | 59.2 | 50.56 | -17.09% | 51.03 | -16.00% | 49.11 | -20.56% |
| FA | 70.3 | 50.77 | -38.47% | 51.24 | -37.20% | 48.74 | -44.23% |
| FA | 12.9 | 19.51 | 33.86% | 20.37 | 36.68% | 20.31 | 36.49% |
| FA | 20.8 | 30.94 | 32.77% | 31.78 | 34.55% | 29.62 | 29.79% |
| FA | 33.3 | 40.74 | 18.27% | 41.45 | 19.65% | 39.63 | 15.98% |
| FA | 46.1 | 43.97 | -4.85% | 44.60 | -3.35% | 42.03 | -9.68% |
| FA | 55.7 | 43.87 | -26.97% | 44.51 | -25.15% | 41.12 | -35.44% |

The figure below is a comparison of the error percentages obtained from the calculation of the three models in the above table. The smaller the error, the more the theoretical value calculated is closer to the actual value measured by the experiment.

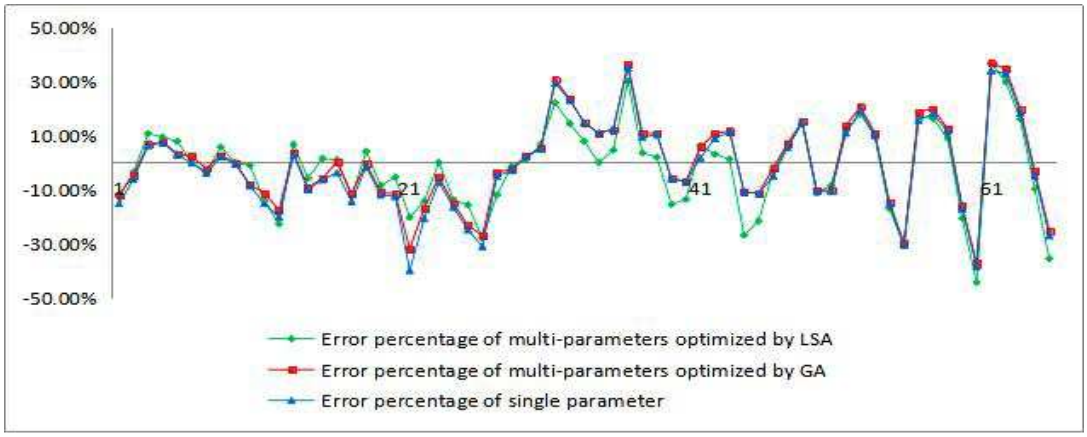


**Fig.1** Comparison of single parameter model and multi-parameter model

It can be seen from the above figure that in the overall data formula of cement with different dosages cement and mineral admixture, when the mineral admixture is steel slag, the main deviation is negative deviation, and the theoretical value obtained is generally higher than the actual value. The value is small, and when the mineral admixture is slag, the main deviation is positive deviation, and the theoretical value obtained is generally larger than the actual value. When the mineral admixture is fly ash, both positive and negative deviations have large errors.

Following the overall model constructed in this paper, several sub-formulas for different admixtures were constructed for different mineral admixtures.

The following table shows the theoretical values obtained from the calculation of the pure cement model. It can be clearly seen that the theoretical value obtained by multi-parameter model calculation is closer to the actual value obtained by the experiment.

**Table 7** Calculation results of pure cement multi-parameter model fitting model

| Identifier | Experimental data | Single parameter | Single parameter percentage error | Multiple parameters (GA) | Multiple parameter percentage error(GA) | Multiple parameters (LSA) | Multiple parameter percentage error(LSA) |
|---|---|---|---|---|---|---|---|
| CO | 35.8 | 36.76 | 2.60% | 36.29 | 1.34% | 35.89 | 0.24% |
| CO | 45.4 | 43.44 | -4.50% | 44.62 | -1.74% | 44.33 | -2.42% |
| CO | 54.4 | 55.20 | 1.46% | 54.49 | 0.17% | 54.40 | 0.01% |
| CO | 55.2 | 56.58 | 2.44% | 55.72 | 0.93% | 55.56 | 0.65% |
| CO | 57.6 | 56.37 | -2.18% | 57.31 | -0.51% | 57.13 | -0.81% |

The figure below is a comparison of the error percentages obtained from the calculation of the three models in the above table. The multi-parameter model has a smaller error in the strength of the cement stone calculated by the single-parameter model, and the value calculated by the mathematical model optimized by LSA is used. Closer to the actual value, the error is kept below 1% when the age is the seventh day. Because the cement hydration rate is weakened on the 7th day, the cement error calculated by the mathematical model is the largest.

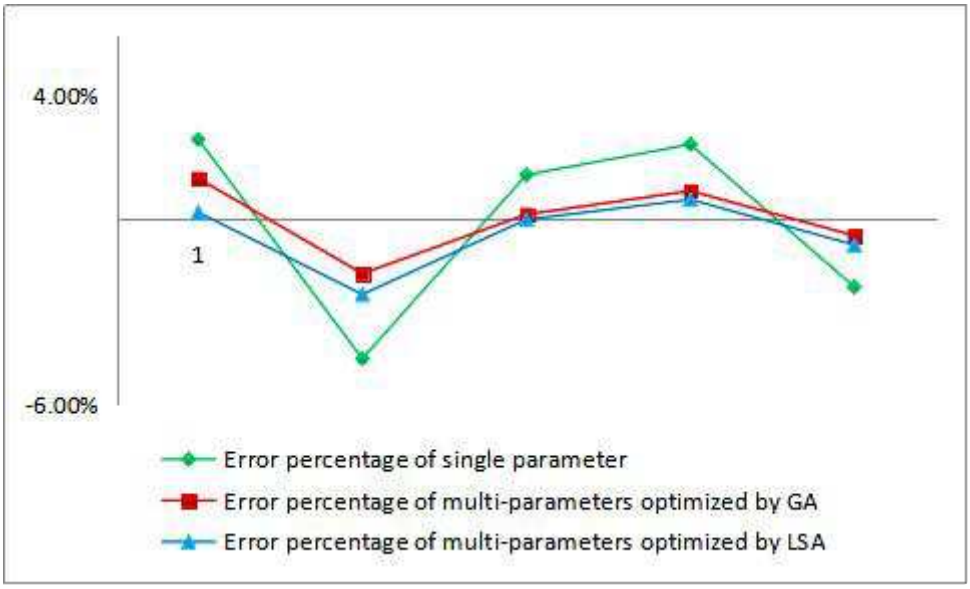


**Figure 2** Comparison of single parameter model and multi-parameter mode

The following table shows the theoretical values obtained by the single-parameter and multi-parameter model calculations for different dosages steel slags. For cements with steel slag, based on the mathematical model constructed by percolation, the theoretical strength of cement is closer to the actual strength of the cement.

**Table 8** Calculation results of multi-parameter model for different dosages steel slag

| Identifier | Experimental data | Single parameter | Single parameter percentage error | Multiple parameters (GA) | Multiple parameter percentage error(GA) | Multiple parameters (LSA) | Multiple parameter percentage error(LSA) |
|---|---|---|---|---|---|---|---|
| C0 | 35.8 | 34.9422 | -2.45% | 35.00 | -2.29% | 35.0086 | -2.26% |
| C0 | 45.4 | 45.2522 | -0.33% | 45.42 | 0.05% | 45.3988 | 0.00% |
| C0 | 54.4 | 59.3502 | 8.34% | 59.80 | 9.04% | 59.5501 | 8.65% |
| C0 | 55.2 | 58.8002 | 6.12% | 59.04 | 6.50% | 59.1435 | 6.67% |
| C0 | 57.6 | 60.4131 | 4.66% | 60.66 | 5.04% | 60.7657 | 5.21% |
| SS1 | 33.3 | 35.9296 | 7.32% | 35.85 | 7.13% | 36.1018 | 7.76% |
| SS1 | 43.2 | 43.2073 | 0.02% | 43.29 | 0.20% | 43.3868 | 0.43% |
| SS1 | 54.4 | 56.6163 | 3.91% | 56.97 | 4.51% | 56.8403 | 4.29% |
| SS1 | 60 | 57.6473 | -4.08% | 57.71 | -3.97% | 58.0952 | -3.28% |
| SS1 | 63.6 | 61.4926 | -3.43% | 62.21 | -2.24% | 61.5508 | -3.33% |
| SS2 | 29.6 | 29.6 | 0.00% | 29.66 | 0.20% | 29.6 | 0.00% |
| SS2 | 42.7 | 37.1875 | -14.82% | 37.23 | -14.70% | 37.315 | -14.43% |
| SS2 | 50 | 53.3732 | 6.32% | 53.71 | 6.90% | 53.5438 | 6.62% |
| SS2 | 60 | 55.7521 | -7.62% | 56.00 | -7.15% | 56.0282 | -7.09% |
| SS2 | 60.1 | 60.1 | 0.00% | 60.86 | 1.25% | 60.1001 | 0.00% |
| SS3 | 23.5 | 27.7295 | 15.25% | 27.75 | 15.32% | 27.7222 | 15.23% |
| SS3 | 38.1 | 36.6245 | -4.03% | 36.62 | -4.06% | 36.756 | -3.66% |
| SS3 | 47.1 | 50.1483 | 6.08% | 50.59 | 6.89% | 50.19 | 6.16% |
| SS3 | 57.6 | 52.8002 | -9.09% | 53.02 | -8.64% | 53.0393 | -8.60% |
| SS3 | 58.8 | 55.8039 | -5.37% | 56.49 | -4.09% | 55.7842 | -5.41% |
| SS4 | 18.1 | 19.884 | 8.97% | 20.07 | 9.81% | 19.6785 | 8.02% |
| SS4 | 32.1 | 31.9602 | -0.44% | 32.12 | 0.06% | 31.9076 | -0.60% |
| SS4 | 44.1 | 46.2204 | 4.59% | 46.72 | 5.60% | 46.1529 | 4.45% |
| SS4 | 54.2 | 48.3069 | -12.20% | 48.45 | -11.88% | 48.5269 | -11.69% |
| SS4 | 57.9 | 51.3875 | -12.67% | 52.13 | -11.08% | 51.2539 | -12.97% |

The following figure shows the comparison of the single-parameter model and the multi-parameter model incorporated into the steel slag. It can be seen from the following figure that the model deviation using LSA optimization mainly occurs when the negative deviation occurs, which is smaller than other models. For cements with steel slag, the values of the constructed percolation-based models are closer to the actual values.

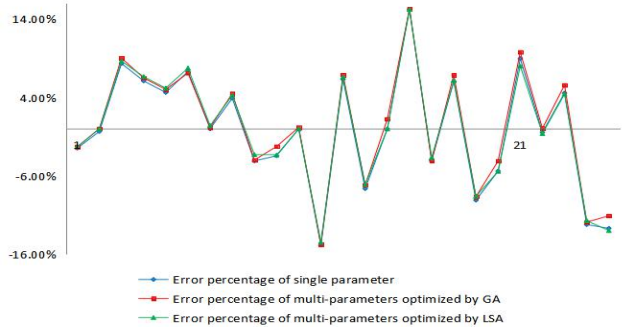


**Figure 3** Comparison of single parameter model and multi-parameter model

The following figure shows the three-dimensional model of the multi-parameter model deviation after LSA optimization. The x-axis represents the age of the cement, the y-axis represents the amount of steel slag, and the z-axis represents the calculated error percentage of the theoretical and actual values. It can be seen that there is a positive deviation at different dosages at 3 and 28 days, and a negative deviation at 7 days, 90 days and 180 days. In the cement with steel slag, the steel slag begins to hydrate early. The hydration characteristics are similar to those of cement. There is no percolation transition of cement-type hydration products such as CSH gel due to the decrease of clinker particles. There is no obvious cohesiveness in the cement stone system; For the pure cement hardened slurry, the porosity data points of the different dosages amounts of steel slag hardened slurry are shifted to the direction of large porosity during the 28-day age period.

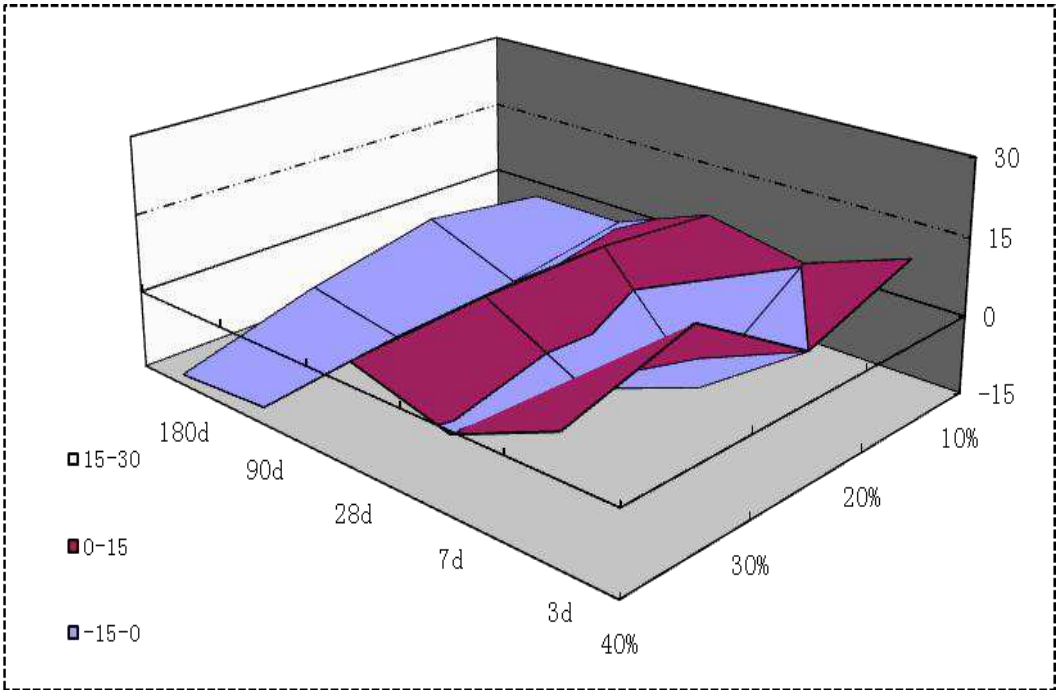


**Figure 4** multi parameter model of steel slag with different dosages

The following table shows the theoretical values obtained by the single parameter model with different dosages slag additions and the multi-parameter model. The percentage error calculated from the theoretical value and the actual measured cement strength.

**Table 9** Calculation results of multi-parameter model of different dosages slag

| Identifier | Experimental data | Single parameter | Single parameter percentage error | Multiple parameters (GA) | Multiple parameter percentage error(GA) | Multiple parameters (LSA) | Multiple parameter percentage error(LSA) |
|---|---|---|---|---|---|---|---|
| C0 | 35.8 | 25.96 | -37.92% | 30.00 | -19.35% | 29.361 | -17.99% |
| C0 | 45.4 | 37.75 | -20.27% | 40.82 | -11.21% | 40.322 | -11.19% |
| C0 | 54.4 | 54.03 | -0.69% | 55.38 | 1.76% | 55.4474 | 1.93% |
| C0 | 55.2 | 55.70 | 0.90% | 56.45 | 2.22% | 56.0962 | 1.62% |
| C0 | 57.6 | 55.45 | -3.88% | 57.98 | 0.66% | 57.6 | 0.00% |

| | | | | | | | |
|---|---|---|---|---|---|---|---|
| SL1 | 36.3 | 22.67 | -60.15% | 27.19 | -33.48% | 26.4209 | -27.22% |
| SL1 | 46.6 | 39.41 | -18.24% | 43.95 | -6.03% | 41.3735 | -11.22% |
| SL1 | 60.3 | 54.63 | -10.39% | 56.56 | -6.61% | 55.609 | -7.78% |
| SL1 | 60.4 | 58.14 | -3.88% | 58.87 | -2.60% | 57.6276 | -4.59% |
| SL1 | 59.7 | 59.30 | -0.67% | 60.56 | 1.42% | 59.68 | -0.03% |
| SL2 | 29.1 | 36.07 | 19.32% | 37.98 | 23.38% | 36.2112 | 24.44% |
| SL2 | 41.8 | 49.90 | 16.23% | 49.47 | 15.50% | 47.3984 | 13.39% |
| SL2 | 56.4 | 63.00 | 10.47% | 62.20 | 9.32% | 59.667 | 5.79% |
| SL2 | 61.8 | 66.66 | 7.29% | 65.40 | 5.51% | 61.8 | 0.00% |
| SL2 | 61.8 | 67.92 | 9.01% | 67.07 | 7.85% | 63.9117 | 3.42% |
| SL3 | 23.3 | 30.59 | 23.82% | 33.77 | 31.00% | 32.1699 | 38.07% |
| SL3 | 37.5 | 36.25 | -3.46% | 39.18 | 4.29% | 37.5 | 0.00% |
| SL3 | 54.2 | 56.63 | 4.29% | 58.30 | 7.03% | 55.0795 | 1.62% |
| SL3 | 68.1 | 60.93 | -11.77% | 60.93 | -11.77% | 58.0639 | -14.74% |
| SL3 | 68.8 | 60.93 | -12.92% | 62.40 | -10.26% | 59.5213 | -13.49% |
| SL4 | 19.7 | 15.48 | -27.25% | 20.59 | 4.34% | 19.7547 | 0.28% |
| SL4 | 34.8 | 33.05 | -5.29% | 36.93 | 5.77% | 35.0412 | 0.69% |
| SL4 | 52 | 54.64 | 4.83% | 57.06 | 8.86% | 53.3423 | 2.58% |
| SL4 | 69 | 58.67 | -17.62% | 60.24 | -14.55% | 55.9077 | -18.97% |
| SL4 | 69.8 | 59.04 | -18.22% | 61.36 | -13.75% | 57.7017 | -17.33% |

The following figure is a comparison of the single-parameter model and multi-parameter model deviation of slag. It can be seen from the following figure that the calculated strength of most multi-parameter models is closer to zero than the single-parameter model. Especially in the negative deviation, the deviation is smaller than the experimental data using the single-parameter mathematical model. It can be seen that for the multi-parameter model, the error is more evenly distributed around 0. There are no particularly large deviations. The intensity value calculated using the LSA-optimized mathematical model is closer to the actual value. In the multi-parameter model, when the slag content is small, the error decreases with time, which indicates that the model has a good effect on cement strength prediction in the old age when the slag content is small.

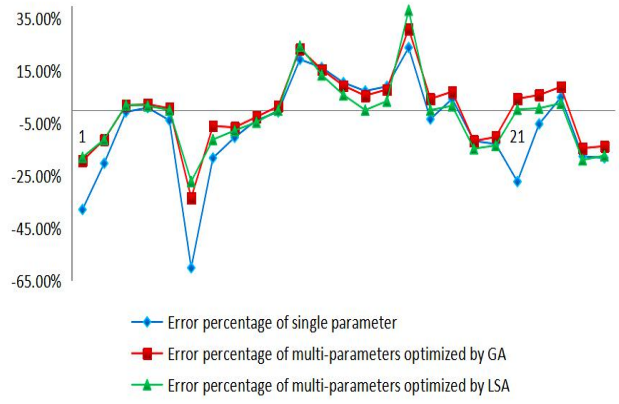


**Figure 5** Comparison of single parameter model and multi-parameter model

The following figure shows a three-dimensional model of multi-parameter model deviation with different dosages slag content after LSA optimization, where the x-axis represents the age of the cement, the y-axis represents the amount of slag, and the z-axis represents the calculated theoretical and actual values. The percentage of error, as can be seen from the three-dimensional graph, the theoretical values obtained in the multi-parameter model at 7 days, 28 days, and 90 days are not much different from the actual values, when the slag content is not high, The theoretical value obtained is also closer to the actual value. The slag can be cemented well in the later stage of hydration.

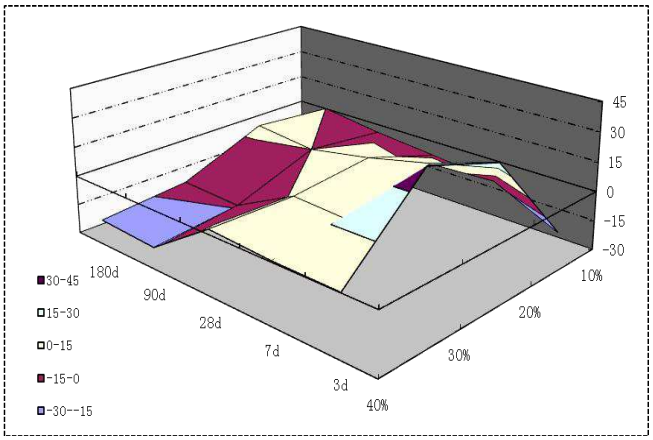


**Figure 6** Three-dimensional map of multi-parameter model of slag with different dosages

The following table shows the theoretical values obtained by the single parameter model with different dosages fly ash additions and the multi-parameter model. The percentage error calculated from the theoretical value and the actual measured cement strength.

**Table 10** Calculation results of multi-parameter model of fly ash with different dosages

| Identifier | Experimental data | Single parameter | Single parameter percentage error | Multiple parameters (GA) | Multiple parameter percentage error(GA) | Multiple parameters (LSA) | Multiple parameter percentage error(LSA) |
|---|---|---|---|---|---|---|---|
| C0 | 35.8 | 22.18 | -61.38% | 27.99 | -27.88% | 26.44 | -35.42% |
| C0 | 45.4 | 37.46 | -21.19% | 41.14 | -10.36% | 39.08 | -16.17% |
| C0 | 54.4 | 61.87 | 12.07% | 59.46 | 8.51% | 54.35 | -0.09% |
| C0 | 55.2 | 64.57 | 14.51% | 61.86 | 10.76% | 59.39 | 7.06% |
| C0 | 57.6 | 64.16 | 10.22% | 63.48 | 9.27% | 60.98 | 5.54% |
| FA1 | 31 | 20.34 | -52.39% | 26.80 | -15.68% | 25.93 | -19.54% |
| FA1 | 40 | 36.90 | -8.40% | 40.74 | 1.81% | 39.73 | -0.68% |
| FA1 | 47.6 | 58.06 | 18.01% | 58.45 | 18.56% | 59.67 | 20.22% |
| FA1 | 64.7 | 62.54 | -3.45% | 62.06 | -4.25% | 63.78 | -1.45% |
| FA1 | 66.4 | 65.34 | -1.63% | 65.14 | -1.93% | 66.40 | 0.00% |
| FA2 | 24.4 | 17.96 | -35.88% | 24.31 | -0.36% | 23.49 | -3.86% |
| FA2 | 32.4 | 33.59 | 3.55% | 38.01 | 14.76% | 37.77 | 14.21% |
| FA2 | 45.8 | 49.90 | 8.21% | 52.67 | 13.05% | 54.26 | 15.59% |
| FA2 | 63.3 | 56.39 | -12.25% | 58.51 | -8.19% | 62.10 | -1.94% |
| FA2 | 71.6 | 56.49 | -26.75% | 58.29 | -22.84% | 60.60 | -18.15% |
| FA3 | 20.5 | 14.78 | -38.73% | 21.07 | 2.73% | 20.21 | -1.45% |
| FA3 | 28.8 | 27.10 | -6.26% | 32.14 | 10.40% | 31.73 | 9.23% |
| FA3 | 41.6 | 43.65 | 4.70% | 48.03 | 13.40% | 50.88 | 18.25% |
| FA3 | 59.2 | 49.34 | -19.98% | 53.45 | -10.76% | 58.02 | -2.04% |
| FA3 | 70.3 | 49.68 | -41.51% | 55.51 | -26.64% | 63.05 | -11.51% |
| FA4 | 12.9 | 10.29 | -25.33% | 16.59 | 22.26% | 15.58 | 17.21% |
| FA4 | 20.8 | 21.99 | 5.40% | 28.07 | 25.91% | 28.60 | 27.26% |
| FA4 | 33.3 | 34.59 | 3.73% | 40.77 | 18.32% | 43.24 | 22.99% |
| FA4 | 46.1 | 39.21 | -17.57% | 46.16 | 0.13% | 51.59 | 10.64% |
| FA4 | 55.7 | 39.06 | -42.59% | 47.60 | -17.01% | 55.70 | 0.00% |

The following figure shows the comparison between the single-parameter model of fly ash and the multi-parameter model deviation. In the single-parameter model based on percolation theory, the deviation is larger on the negative deviation, and the deviation from the other models is smaller on the positive deviation, but Due to the excessive deviation of the negative deviation, the overall model prediction effect is not good. When the negative deviation error is large, it is mainly on the 3rd and 90th days. The new mathematical model constructed in this paper effectively solves the problem of large negative deviation. Not only the deviation of most data is closer to 0 than the single-parameter model, but also the deviation is basically about plus or minus 20%, which is more realistic.

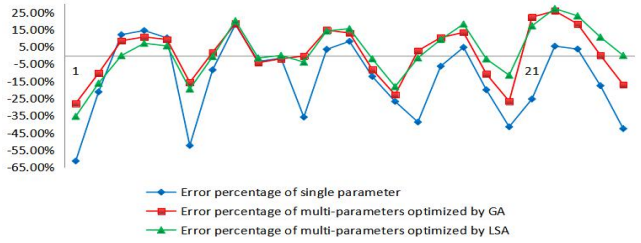


**Figure 7** Comparison of single parameter model and multi-parameter model

The following figure shows the multi-parameter model deviation of the mixed fly ash with LSA optimization, where the x-axis represents the age of the cement, the y-axis represents the amount of fly ash, and the z-axis represents the calculated theory. The percentage error between the value and the actual value can be seen from the three-dimensional graph. As the amount of fly ash increases, the deviation of the obtained cement strength gradually becomes larger. When the cement hydration is early and the cement hardened slurry is stable, the strength of the obtained cement is closer to the actual value, and at around 28 days, the obtained cement strength deviates more from the actual value.

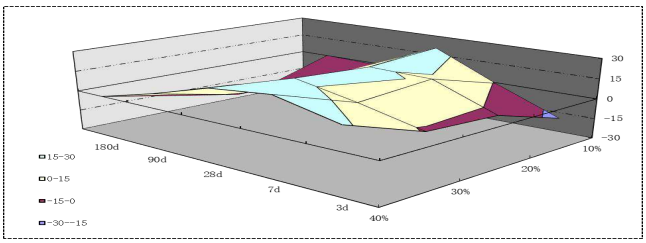


**Figure 8** Three-dimensional map of multi-parameter model of fly ash with different dosages

The cement stone microstructure model based on percolation theory is considered to be the problem of multi-color percolation in the dispersed reinforcing phase, dispersed degraded phase and continuous phase in its space, which lays a foundation for the quantitative characterization of the relationship between the microstructure of cement-based materials and its macroscopic properties. Conducive to the understanding and control of the performance of cement-based materials. In ordinary cement stone, the percolation path of the hole has appeared, and its macroscopic mechanical properties are mainly related to the spatial connection degree of the hole. When constructing the cement stone porosity strength model, the degree of percolation of the hole should be reflected in the mathematical solution of the model. Porosity has a direct influence on the strength of cement stone, while CH, total bound water and gel-bound water also have a certain influence on the strength of cement stone.

## 4. Conclusion

This paper uses CH, total bound water, gel combined with water and porosity to construct together. The model is used to calculate the strength of cement stone. The experimental results show that the multi-parameter model constructed in this paper has a higher degree of fit than several commonly used porosity-strength models, compared to the single-parameter porosity-strength model based on pore percolation. The calculated intensity is closer to the actual value. Through the optimization algorithm, it can iteratively optimize and optimize its coefficients, improve the fitting effect, and have a certain lifting space. The lightning search algorithm performs iterative optimization to fit the multi-parameter numerical formula to better predict the mechanical properties of the material.Would it be better to use the current popular deep learning algorithms? This will require further research.

## CRediT authorship contribution statement

**Wei Liu:** Writing-review & editing. **Xuguang Wu:** Writing-review & editing. **Yingbin Wang**: Data curation. **Zhiwei Ye:** Conceptualization, Methodology. **Pan Li:** Software.

## Declaration of Competing Interest

The authors declare that they have no known competing financial interests or personal relationships that could have appeared to influence the work reported in this paper.

## Acknowledgments

This research is supported by the National Natural Science Foundation of China (61772180, 61602162, 52008158), technological innovation project of Hubei province2019(2019AAA04), the Hubei provincial Natural Science Foundation of China (2015CFB594), State Key Laboratory of Geo-Information Engineering (SKLGI 2014-M-3-3), and the Green Industry Leadership Program of Hubei University of Technology (YXQN2017002).

## References

J. Zallen, R . (2007) The physics of amorphous solids. https://doi.org/10.1002/9783527617968

Hammersley J M, Handscomb D C(1957) Percolation Processes. Mathematical Proceedings of the Cambridge Philosophical Society . 53(3):629-641

Kearsley E P, Wainwright P J(2002) The effect of porosity on the strength of foamed concrete. Cement & Concrete Research . 32(2):233-239

Pandey S P, Sharma R L (2000) The influence of mineral additives on the strength and porosity of OPC mortar. Cement & Concrete Research .30(1):19-23

Baoguo Ma (2005) Influences of a New Admixture MX on Concrete Durability . Journal of Wuhan University of Technology-Materials Science. https: //doi.org/10.1007/BF02870891

Yongxin Li (2003) Microstructure and Composition of Hydration Products of Ordinary Portland Cement with Ground Steel-making Slag . Journal of Wuhan University of Technology-Materials Science. 04:76-79

Grabois T M, Cordeiro G C, Filho R D T(2018) The Influence of Recycled Concrete and Clay Brick Particles on the Strength and Porosity of Cement-Based Pastes. https://doi.org/10.1007/978-94-024-1207-9_30

Zajac M, Skocek J, Adu-Amankwah S, et al (2018) Impact of microstructure on the performance of composite cements: Why higher total porosity can result in higher strength . Cement & Concrete Composites. https:// doi. org/ 10.1016/j.cemconcomp.2018.03.023

Peng Zhao,WeiHe Wang (2008) The Microcosmic Modality of Fly Ash and its Characteris- tic in Cement Hydration . Fly Ash Comprehensive Utiliz- ation

Zhao Z, Du C W, Shen L(2013) Correlation Test between Resistivity and Microcosmic Pore Structure of Mineral Admixture Concrete. Applied Mechanics & Materials. 438-439 : 75-80.https:/ /doi.org/10.4028/www. scientific.net/AMM.438-439.75

Constantinides G, Ulm F J(2004) The effect of two types of C-S-H on the elasticity of cement-based materials: Results from nanoindentation and micromechanical modeling. Cement & Concrete Research . 34(1):67-80

Wang L, Yang H Q, Zhou S H, et al (2018) Hydration, mechanical property and C-S-H structure of early-strength low-heat cement-based materials. Materials Letters . 217

Land G, Stephan D(2018) The effect of synthesis conditions on the efficiency of C-S-H seeds to accelerate cement hydration . Cement & Concrete Composites . 87 : 73 -78. https://doi.org/10.1016/j.cemconcomp.2017.12.006

Borges P H R, Costa J O, Milestone N B, et al(2010) Carbonation of CH and C–S–H in composite cement pastes containing high amounts of BFS . Cement & Concrete Research.40(2):284-292.https://doi.org/10.1016/j. cemconres. 2009.10.020

M.Elsisi(2022)Improved grey wolf optimizer based on opposition and quasi learning approaches for optimization: case study autonomous vehicle including vision system.Artificial Intelligence Review.1-24.https://doi.org/10.1007/s10462-022-10137-0

Mahmoud Elsisi,Minh-Quang Tran,Hany M. Hasanien,Rania A. Turky,Fahad Albalawi,Sherif S. M. Ghoneim(2021)Robust Model Predictive Control Paradigm for Automatic Voltage Regulators against Uncertainty Based on Optimization Algorithms.Mathematics.9(22):2885.https://doi.org/10.3390/math9222885

M. Elsisi,Mohamed A. Ebrahim(2021)Optimal design of low computational burden model predictive control based on SSDA towards autonomous vehicle under vision dynamics. International Journal of Intelligent Systems. 36(11): 6968-6987. https://doi.org/10.1002/int.22576

M.Elsisi,Mohamed A. Ebrahim(2021) Optimal design of nonlinear model predictive controller based on new modified multitracker optimization algorithm.International Journal of Intelligent Systems.35(11):1857-1878. https://doi.org/10.1002/int.22275

SHAREF H,IBRAHIM A A, MUTLAG A H(2015) Lightning search algorithm. Applied Soft Computing.36(S): 315-333. https://doi.org/10.1016/j.asoc.2015.07.028

Ammar M, Mohamed A, Abubarkr H(2020) Optimal Sizing and Location of Solar Capacity in an Electrical Network Using Lightning Search Algorithm . Neuro Computing. 04: 4-5.https://doi.org/10.1080/1532 5008.2019. 1659 456

Mohammed W, Awartni-Ghaith M, Oujda K(2020) Chaotic lightning search algorithm.Soft Computing. https: //doi.org/10.1007/s00500-020-05273-0

Ashish-Kumar B, NehaSingh, Immadisetty-Vinod K(2020) Lightning Search Algorithm-based Contextually Fused Multilevel Image Segmentation. Applied Soft Computing, 2020. https://doi.org/10.1016/j.asoc.2020.106243

ArupRantan, AjoyKumar - Chakraborty(2019) Probabilistic Load Flow Based Optimal Sizing and Placement of DG and DSTATCOM Using Chaotic Lightning Search . Iceeccot.IEEE.https://doi.org/10.1109/ICEECCOT46775.2019.9114853

W.M.Hamanah, M.A.Abido, Luai M(2019) Optimum Sizing of Hybrid PV, Wind, Battery and Diesel System Using Lightning Search Algorithm. Arabian Journal for Science and Engineering.https://doi.org/10.1007/s1 3369-019-04292-w

M. Elsisi, H. Abdelfattah(2020) New design of variable str - ucture control based on lightning search algorithm for nuclear reactor power system considering load-following operation.Nu-clear Engineering and Technology .https://doi.org/10.1016/j.net.2019.08.003 .

Serhat Duman(2019) Solution of the Optimal Power Flow Problem Considering FACTS Devices by Using Lightning Search Algorithm.Iranian Journal of Science and Technol- ogy Transactions of Electrical Engineering.https://do i.org/ 10.1007/s40998-019-00199-2.